Mon. Not. R. Astron. Soc. **367,** 815–824 (2006) doi:10.1111/j.1365-2966.2005.09992.x

GMOS spectroscopy of the S0 galaxy NGC 3115

Mark A. Norris,[1⋆] Ray M. Sharples[1] and Harald Kuntschner[2]

[1]*Department of Physics, Science Laboratories, South Road, Durham*
[2]*Space Telescope European Coordinating Facility, European Southern Observatory, Karl-Schwarzchild-Str. 2, 85748 Garching, Germany*

Accepted 2005 December 15. Received 2005 December 13; in original form 2005 October 6

ABSTRACT

We present Gemini Multi-Object Spectrograph longslit spectroscopy of the isolated S0 galaxy NGC 3115. We have determined kinematical data and Lick/IDS absorption line-strength indices for the major axis out to around 9 kpc and for the minor axis out to around 5 kpc (around $2R_e$). Using stellar population models which include the effects of variable [α/Fe] ratios, we derive metallicities, abundance ratios and ages for the stellar population of NGC 3115. We find that [α/Fe] remains fairly constant with increasing radius at around [α/Fe] = 0.17 for the major axis but increases rapidly for the minor axis to around [α/Fe] = 0.3. We also find that to first order, this behaviour can be explained by a simple spheroid + disc model, where the spheroid has [α/Fe] = 0.3 and the disc shows close to solar abundance ratios. The disc also appears considerably younger than the spheroid, having an age of around 6 Gyr compared to 12 Gyr for the spheroid. We compare these results to those previously presented for the globular cluster system of NGC 3115.

Key words: galaxies: abundances – galaxies: general – globular clusters: general – galaxies: stellar content – galaxies: individual: NGC 3115.

1 INTRODUCTION

Globular clusters (GCs) are among the simplest stellar systems. The stellar content of individual clusters form primarily at one epoch and location, and so are remarkably uniform in terms of metallicity, age and chemical abundances. Because GCs are believed to form preferentially during the major star-forming and mass accumulation epochs, a careful examination of the GC population of a galaxy can shed light on these periods of a galaxy's development. However, this relies on the assumption that GCs act as good tracers of the properties of the overall stellar population formed at the same epoch. For a more thorough discussion of why this is believed to be the case, see Puzia et al. (2005). The aim of the present work is to test this hypothesis in detail for one well-studied galaxy.

NGC 3115 (see Table 1) is one of the closest and most studied S0 galaxies. Its GC system has been extensively investigated, using both photometric (Kavelaars 1998; Kundu & Whitmore 1998; Puzia et al. 2002) and spectroscopic (Kuntschner et al. 2002; Puzia et al. 2004) techniques. These studies find two GC subpopulations of mean metallicities [Fe/H] $\simeq -0.37$ and [Fe/H] $\simeq -1.36$. Kuntschner et al. (2002) find that both GC subpopulations have ages which are consistent with a single epoch of formation about 12 Gyr ago. The observations of Kundu & Whitmore (1998) and Kavelaars (1998) are consistent with the metal-rich clusters being associated with a rapidly rotating thick disc system and the slower rotating metal-poor clusters being associated with the halo of NGC 3115. The stellar population of the galaxy itself has also been examined, notably by Fisher, Franx & Illingworth (1996) who measured the line strengths and their gradients out to a radius of 40 arcsec along the major axis; Trager et al. (1998) also examined the absorption-line indices of the galaxy nucleus. Elson (1997) found evidence for a bimodal distribution of metallicities with [Fe/H] $\simeq -0.7$ and [Fe/H] $\simeq -1.3$ in the resolved stellar population of the halo located 8.5 arcmin east of the centre and 5 arcmin from the major axis, although Kundu & Whitmore (1998) suggested that this might be due to an instrumental effect in the metallicity calibration. Taken together, these observations lead to the possibility that the metal-poor subpopulation formed 12–13 Gyr ago, with the metal-rich population forming several Gyr later after the interstellar medium has been enriched by a factor of $\simeq$4, perhaps triggered by active galactic nucleus activity or a merger event. A further examination of the ages and metallicities of the general stellar population and the GC population in this galaxy using updated Simple Stellar Populations (SSP) models can test the plausibility of these scenarios.

This paper is structured as follows. Section 2 describes the data set and its reduction; Section 3 discusses the kinematical results of this investigation and Section 4 examines the line indices and their use for calculation of luminosity-weighted abundance ratios, age and metallicity. Section 5 describes a simple two-component fit to the [α/Fe] ratios of NGC 3115, Section 6 includes a general discussion of the results of the previous sections and Section 7 presents our conclusions.

⋆E-mail: m.a.norris@durham.ac.uk (MAN)

Table 1. NGC 3115 basic parameters.

Parameter	Value	Source
Right ascension (J2000)	$10^{h}05^{m}13.98^{s}$	*a*
Declination (J2000)	$-07^{\circ}43'06''.9$	*a*
Morphological type	$S0^{-}$	*a*
Major diameter	7.2 arcmin	*a*
Minor diameter	2.5 arcmin	*a*
Heliocentric radial velocity	$663 \pm 4\,\mathrm{km\,s^{-1}}$	*b*
Asymptotic radial velocity	$263 \pm 5\,\mathrm{km\,s^{-1}}$	*b*
Central velocity dispersion	$314 \pm 4\,\mathrm{km\,s^{-1}}$	*b*
Inclination of disc	86°	*c*

[a]NASA/IPAC extragalactic database (NED). http://nedwww.ipac.caltech.edu/.
[b]This study.
[c]Capaccioli et al. (1993).

2 OBSERVATIONS AND DATA REDUCTION

The observations were carried out on 2001 December 18/19 with the Gemini Multi-Object Spectrograph (GMOS) instrument (Hook et al. 2004) on the Gemini North Telescope (Program ID GN-2001B-Q-44). The B600 grism with 600 lines per mm was used with a longslit 1-arcsec wide by 335-arcsec long. The data were binned by 4 in the spatial dimension and 2 in the spectral dimension producing a spectral resolution of ∼4.4 Å full width at half-maximum (FWHM) (110 km s^{-1}) sampled at 0.9 Å pixel^{-1}. The seeing throughout the observations was generally $\leqslant$0.8 arcsec, and the binned pixel scale was 0.3 arcsec pixel^{-1}. The wavelength range was ∼3800–6400 Å. Two sets of integrations were completed, one each for the major and minor axis of the galaxy, with a total integration time for each axis of 7200 s. The centre of the major axis longslit was offset from the galaxy centre along the major axis by 120 arcsec, as can be seen in Fig. 1, to extend the radial coverage and reduce the galaxy light in the sky background region. For the minor axis, the sky region was defined at either end of the longslit. As can be seen from Fig. 1, the sky-subtraction regions are located at large radii where the galaxy flux is only 5-6 per cent of the sky level, hence over-subtraction of galaxy light should not be a major problem. This is discussed in more detail in Section 2.1. Two velocity standards HD97907, HD73665 and a photometric standard Feige 34 were also observed using the same experimental set-up.

The standard Gemini IRAF routines were used to carry out bias subtraction, flat-fielding and cosmic ray subtraction. In addition to these procedures, it was noted that scattered light seriously compromised the measurement of line indices at large galactocentric radii. The scattered light had the effect of decreasing measured line indices by applying a constant offset to the spectra; this effect leads to the measurement of spurious age gradients at large radii. Fortunately, the GMOS set-up utilized in this investigation provided the opportunity to remove this scattered light. This was possible because the 2D spectrum produced contained three unexposed regions created by the bottom of the slit and two slit spacers located at 1/3 and 2/3 of the distance along the spatial dimension of the image. After bias subtraction, these regions should contain no flux; however light scattered within the spectrograph meant that this was not the case. To correct for this effect, it was possible to interpolate the scattered light level between the three unexposed regions and to subtract this from the image. In total, scattered light accounted for ∼ a few per cent of the total incident light. However, this was sufficient to account for ∼50 per cent of the counts at the largest radii. After correction, residual scattered light should be of a negligible level.

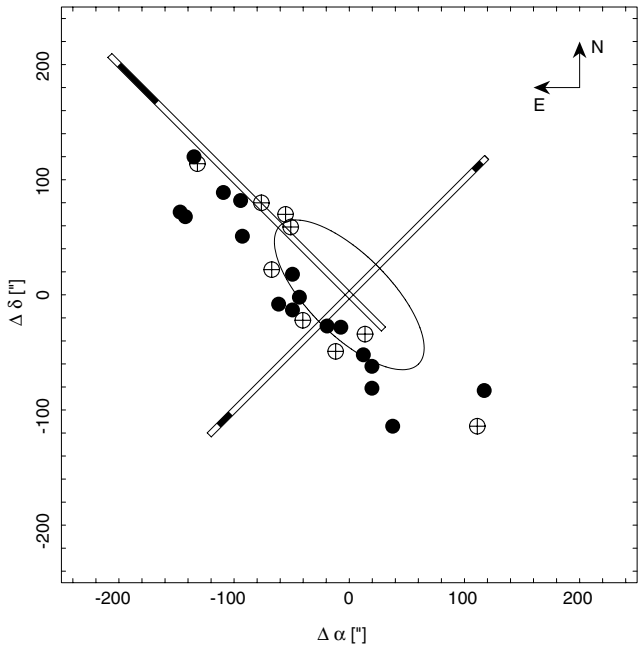

Figure 1. Positions of the major and minor axis longslits. Slit widths exaggerated by a factor of 5. Dark regions define sky-subtraction regions. Filled circles denote positions of GCs examined by Kuntschner et al. (2002) with line-index measurements, unfilled circles have only kinematical data from Kuntschner et al. (2002) available. The ellipse indicates the position and orientation of the galaxy and encloses roughly half the integrated light (Michard & Marchal 1994).

The data were then wavelength calibrated with the wavelength calibration being accurate to $\leqslant$0.2 Å. The 2D spectrum was then extracted into a series of 1D spectra which were sky subtracted and binned in the spatial dimension until the target signal-to-noise ratio (S/N; measured in a region near to the Hβ line) of 20 or 60 (see Section 3) was reached. After binning to S/N = 60, a total of 108 (major axis) and 44 (minor axis) spectra were produced, it is from these spectra that all of the kinematics and line indices were measured, though in later figures these have been rebinned in groups of four (radially) to allow clearer presentation. The binned 1D spectra were then flux calibrated using the photometric standard and a reddening correction of $E(B-V) = 0.146$ (Schlegel, Finkbeiner & Davis 1998) applied using the standard IRAF routines.

2.1 Sky Subtraction

Clearly, an accurate sky subtraction is a necessity when attempting to measure accurate kinematics and line indices at large galactocentric radii. If the sky spectrum is strongly contaminated by diffuse stellar light, it can introduce large errors in measured indices and kinematic quantities, such as σ, h_3 and h_4. To investigate the magnitude of this effect several methods were used, the simplest of which was to re-reduce our data using the minor axis sky to sky subtract the major axis and vice versa. The line indices were remeasured and compared to those measured previously; for all indices considered here the changes in measured index were <0.1 Å except for the Mg *b* line which showed quite considerable variation. This change in the Mg *b* line can be understood as being entirely due to changes in the strength of the 5200 Å sky emission feature between the major and the minor axis exposures.

The second test carried out was to reduce the data assuming ±20 per cent errors in the sky spectra, again any changes in the measured indices were <0.1 Å for all cases except for the very last (and largest) radial bin. We are therefore confident that errors introduced by the sky subtraction should be entirely negligible for all but the very largest (and most binned) radial bins.

2.2 Kinematics

The first step in analysing the spectra was to measure the line-of-sight velocity distribution (LOSVD) for each of the binned spectra. The publicly available IDL implementation of the pPXF method (Cappellari & Emsellem 2004) was employed to determine the recessional velocity, velocity dispersion and the Gauss–Hermite moments h_3 and h_4 for the individual spectra. In this method, the NGC 3115 spectra were fit in pixel space over the wavelength range 4900–5450 Å using both the stellar velocity templates observed during the run and the additional stellar templates from the library of Vazdekis (1999). Errors were estimated by remeasuring 100 Monte Carlo simulations of the spectra with added photon noise. Additionally, as a check of accuracy, the redshift and velocity dispersion were measured by Fourier cross-correlating the spectra against the velocity standards using the FXCOR implementation in IRAF. As the two methods produce consistent results, the more comprehensive pPXF implementation was used for the remaining analysis.

2.3 Line indices

The system of line-strength indices, most commonly used for optical studies, is the Lick/IDS system (Worthey & Ottaviani 1997; Trager et al. 1998). We convolve our spectra with a wavelength-dependent Gaussian kernel to reproduce the Lick/IDS resolution of ∼9–11 Å.

The line-strength indices were then measured for each spectrum and corrected for the smearing effects of the LOSVD following the procedure of Kuntschner (2004). This procedure corrects the line-index measurements for the effects of velocity dispersion and the non-Gaussian h_3 and h_4 terms. Kuntschner (2004) finds that for changes of ±0.1 in h_4 with constant $\sigma = 250\,\mathrm{km\,s^{-1}}$, the LOSVD correction changes by ± 5 per cent with corresponding errors in the age and metallicity estimations of 15–20 per cent. Clearly, for a galaxy such as NGC 3115, with central velocity dispersion of around $300\,\mathrm{km\,s^{-1}}$, the effect of these corrections on the spectra from the central few arcsec could be non-negligible. We therefore only measure indices for which Kuntschner (2004) has provided corrections for these effects (17 indices) though in practice we only make use of the $H\delta_A$, $H\gamma_A$, $H\beta$, Fe5015, Mg b Fe5270 and Fe5335 indices in the following analysis. Errors in the line indices were calculated by 500 Monte Carlo simulations of the input spectra.

Because of the limited number of stars in the Lick library observed during the course of the observations, an accurate determination of the offsets (see e.g. Kuntschner 2000) between line indices measured here and the Lick system could not be determined empirically. However, we made use of the stellar library observed by Jones (1997) to determine the offsets for indices measured on flux- calibrated spectra to the original Lick/IDS system assuming that the Jones library is well flux-calibrated. The spectra were first broadened to the Lick/IDS resolution with a wavelength-dependent Gaussian assuming a spectral resolution of the Jones library of 1.8-Å FWHM. Then, we compared the index measurements in common with the Lick stellar library (Worthey et al. 1994) for up to 128 stars depending on the availability of the measurements. The offsets and associated errors (see Table 2) were derived with a biweight estimator. The offsets are generally small (< 0.1 Å) but individual indices can show larger offsets (e.g. $H\gamma_A$, Fe5015). Here, we have only considered a single offset per index and ignored possible trends with line strength. Several indices (e.g. $H\delta_A$, CN_2, G4300) show weak evidence for such trends which are, however, difficult to quantify (see also Vazdekis 1999). Our determination of the Lick offsets derived from Jones stars is in excellent agreement with an earlier investigation carried out by Worthey & Ottaviani (1997, table 9). For the present study, we apply the offsets listed in Table 2. Typical rest-frame spectra are shown in Fig. 2.

Table 2. Offsets to the Lick/IDS system derived from Jones (1997) library.

Index	Offset	Number of stars
$H\delta_A$	-0.36 ± 0.05 Å	108
$H\delta_F$	-0.16 ± 0.03 Å	110
CN_1	0.003 ± 0.002 mag	117
CN_2	0.006 ± 0.002 mag	115
Ca4227	0.00 ± 0.02 Å	126
G4300	-0.28 ± 0.04 Å	128
$H\gamma_A$	0.38 ± 0.04 Å	126
$H\gamma_F$	0.09 ± 0.02 Å	126
Fe4383	0.28 ± 0.05 Å	126
$H\beta$	-0.12 ± 0.02 Å	128
Fe5015	0.23 ± 0.04 Å	126
Mg b	-0.08 ± 0.02 Å	128
Fe5270	-0.07 ± 0.02 Å	128
Fe5335	-0.04 ± 0.03 Å	128
Fe5406	-0.06 ± 0.02 Å	126

Note. Column (1) gives the index name, while column (2) gives the mean offset (Lick–Jones) to the Lick/IDS system evaluated from the Jones (1997) stars in common with Lick. Column (3) shows the number of stars used in the comparison.

Table 3. Major axis kinematics.

Radius (arcsec)	Velocity ($\mathrm{km\,s^{-1}}$)	σ ($\mathrm{km\,s^{-1}}$)	H_3	H_4
−130.71	229.33	106.66	−0.098	0.013
±	4.15	5.49	0.008	0.007
−78.66	245.07	98.98	−0.158	−0.028
±	7.9	8.98	0.017	0.014
−70.52	244.13	98.48	−0.140	−0.062
±	8.04	10.53	0.018	0.017
−64.41	242.45	106.53	−0.122	−0.008
±	8.29	9.1	0.017	0.013
−59.47	242.97	101.13	−0.147	−0.012
±	8.68	8.88	0.019	0.013
−55.11	242.83	104.85	−0.175	−0.018
±	7.97	9.24	0.017	0.014

Note. Table continued in electronic format. Tables 4 (minor axis kinematics), 5 and 6 (major and minor axis line strengths, ages, [α/Fe] and [Z/H]) are provided in electronic form. All data provided in Tables 3–6 from spectra binned to S/N of 60.

3 GALAXY KINEMATICS

Fig. 3 and Tables 3 and 4 display the results of the kinematical measurements, the velocity measurements are based on spectra binned to have S/N = 20, the other parameters were derived from spectra binned to have S/N = 60. As a check that changes in S/N do not affect the measured quantities, the data were rebinned to S/N of 30,

40 and 50; the kinematics were then remeasured with no significant trends in measured quantities being observed.

We will discuss each of the parameters measured here in turn, but in general the measured kinematical data are in very good agreement with published data from several authors including Kormendy & Richstone (1992), Capaccioli et al. (1993), Bender, Saglia & Gerhard (1994) and Fisher (1997) in almost all respects except for the inferred h_4 value and the rotational velocity at large radii.

The inner rotation curve of the major axis measured here is in good agreement with all the data sets we have examined including Illingworth & Schechter (1982), Kormendy & Richstone (1992), Capaccioli et al. (1993), Bender et al. (1994), Fisher (1997) and Emsellem, Dejonghe & Bacon (1999). At larger radii, however, other authors including Capaccioli et al. (1993) have measured an essentially flat rotation curve with rotational velocity around 260 km s^{-1}. We, however, observe some evidence for some drop off beyond 70 arcsec. As observed by several authors, we find no evidence for minor axis rotation. Statistics are insufficient at present to determine if either of the GC subpopulations can be better associated with structures such as discs or spheroids within NGC 3115. It is, however, clear that the bulk of the clusters examined rotate in a manner consistent with that of the bulk of the stellar content even at larger radii. In fact, of the 26 clusters with kinematics examined here 21 rotate in a prograde manner.

The velocity dispersion of NGC 3115 is also in good agreement with other measured results from the authors cited previously. However, the data we present here extend to significantly larger radii than previous studies. One obvious feature of the data presented in Fig. 3 is that the minor axis velocity dispersion is considerably higher than that of the major axis at equivalent radii. The fact that the minor axis data display a higher velocity dispersion than the major axis is not entirely unexpected as data presented by Kormendy & Richstone (1992) hint at this being the case. The 2D spectroscopy presented in Emsellem et al. (1999) also displays evidence for lines of constant velocity dispersion being elongated in the minor axis direction (at least within the inner 5 arcsec). A difference in measured velocity dispersion for the major and minor axes can be explained if the galaxy consists of a fast-rotating, kinematically cool disc component and a slower rotating, kinematically hot spheroidal component. This possibility is re-examined later in the light of line index measurements.

The values of h_3 determined here are entirely consistent with values determined previously.

The h_4 values measured here are generally consistent with those measured previously except at larger radii, where we observe a value h_4 of 0.0, but Bender et al. (1994) find a value of around 0.1; this discrepancy could be due to several factors including differing experimental set-up and method of measuring h3 and h4.

4 LINE INDICES

4.1 Abundance ratios

In Fig. 4, we show Mg b versus ⟨Fe⟩ where ⟨Fe⟩ = [(Fe5270 + Fe5335)/2] (González 1993), for the major and minor axes of NGC 3115. The GC data points are separated into red and blue subpopulations by $(V - I)$ colour. Model predictions from Thomas, Maraston & Korn (2004) are over-plotted for [α/Fe] of 0.0, 0.3 and 0.5 with ages = 3 (left most line in each group), 5, 8 and 12 (right most line in each group) Gyr and have [Z/H] which ranges from −2.25 (bottom left) to +0.35 (top right). The effects of age and metallicity are essentially degenerate in this diagram, with sensitivity to abundance ratios maximized. As described in Kuntschner et al. (2002), abundance ratios are most accurately determined for larger ages/metallicities.

The measurements for the centre of NGC 3115 from the major axis data are in reasonable agreement with those from Fisher et al. (1996) and also from Trager et al. (1998). The implied α-element over-abundance of [α/Fe] ≈ 0.17 was determined by χ^2 minimization of the data and the models of Mg b versus ⟨Fe⟩ from Thomas et al. (2004). This χ^2 procedure, which is similar to the one introduced by Proctor, Forbes & Beasley (2004), fits the set of indices used here (Hβ, Fe5015, Mg b Fe5270 and Fe5335) to the models of Thomas et al. (2004), allowing variable ages, [α/Fe] and [Z/H]. A possible break in the value of [α/Fe] is visible for Mgb < 4 with an increase in [α/Fe] to around 0.25. In comparison, the minor axis data start off at values consistent with the central portion of the major axis, and then begin to trend off towards [α/Fe] = 0.3 much more rapidly.

A break in the major axis data and differences between the two axes can be interpreted as evidence for the existence of at least two distinct populations, with typical values of [α/Fe] $\sim$ 0.17 and 0.3.

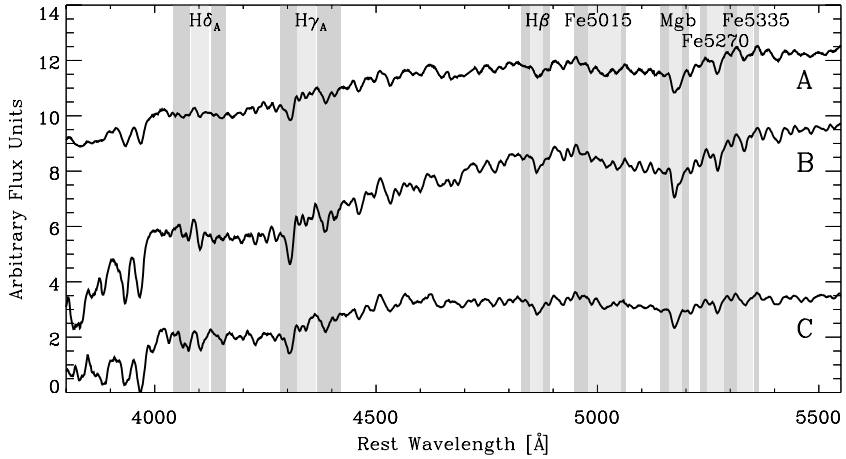

Figure 2. Typical rest-frame spectra corrected to the Lick/IDS resolution obtained in this study. Spectrum A is from the central region, Spectra B and C are the largest radii spectra from the major (≈130 arcsec) and minor axes (≈70 arcsec), respectively. Over-plotted are the index bands (light grey) and red/blue continua (dark grey) for the main Lick indices measured in this study.

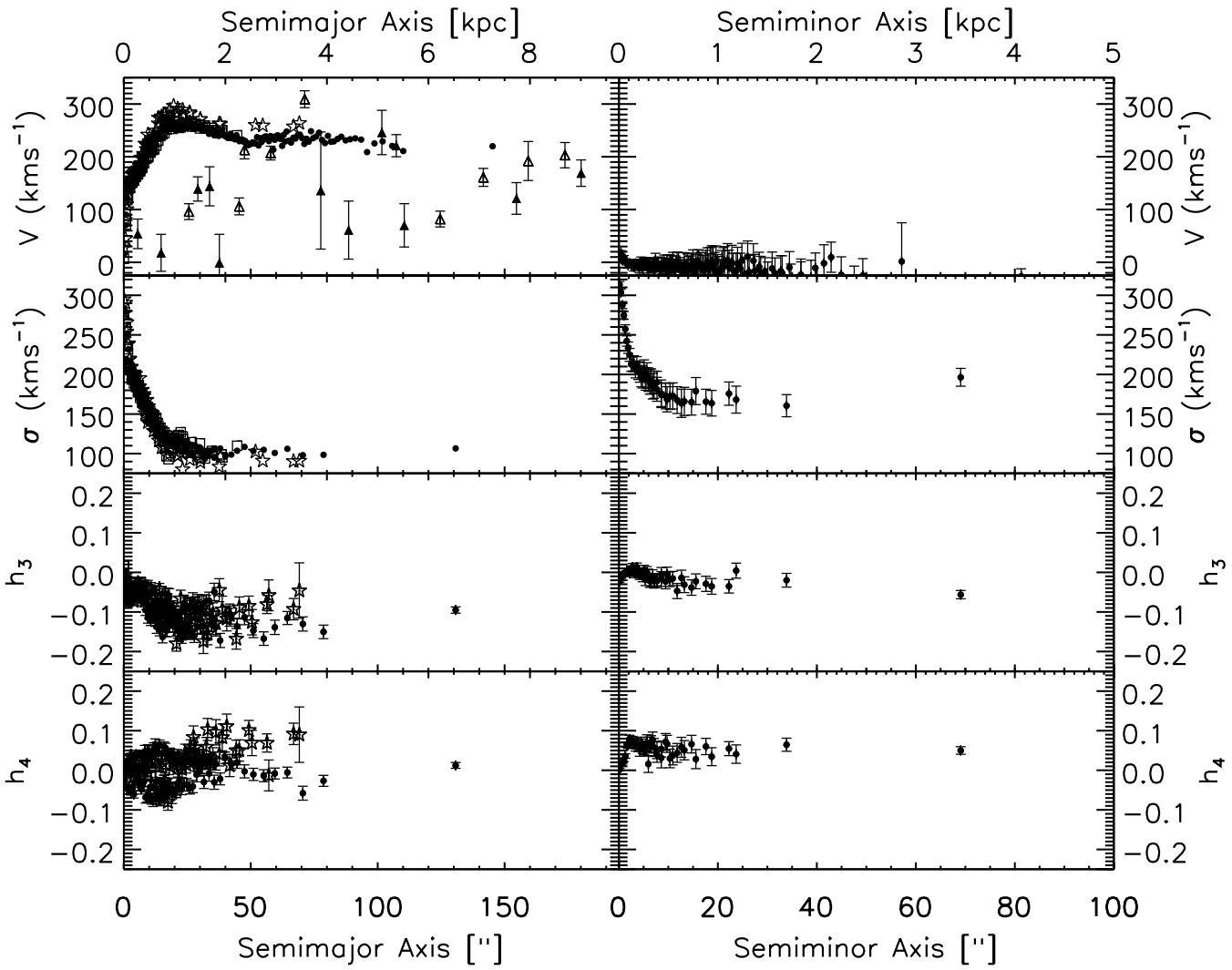

Figure 3. Comparison of measured LOSVD parameters with literature values. Filled circles are from this study, asterisks from Bender et al. (1994) and squares from Fisher (1997). Triangles show GC data from Kuntschner et al. (2002) de-projected to the major axis; filled triangles are the blue subpopulation and unfilled the red subpopulation. Several GC points are omitted because they exhibit counter rotation or have implied rotation velocities of greater than 400 km s^{-1}. Bootstrapped 1σ error bars are over-plotted for values determined in this study, except for major axis velocity and velocity dispersion data where they are omitted in the interests of clarity. Typical errors in V and σ are $\leqslant$12 km s^{-1}. The major axis data have been mirrored about the minor axis and about the central recessional velocity, the minor axis has similarly been mirrored about the major axis.

Since a move towards lower Mg b and ⟨Fe⟩ corresponds to a move to increasing radius, it raises the possibility of observing radial trends in the strengths of other line indices, which will be examined in more detail in the next section.

Our data extend to sufficiently large radii that the mean metallicity of the stellar population is similar to that of the most *metal-rich* GCs. Fig. 4 shows that on both the major and the minor axis, the mean abundance ratios at the largest radii are also consistent with those of the cluster population although the spread in abundance ratios appears to be smaller. No significant population of GCs are found with properties similar to the stellar population at intermediate radii on the major axis.

4.2 Radial profiles of indices

Fig. 5. displays the radial profiles of the measured Lick indices, [α/Fe] and [Z/H]. The values of r_e used here are those listed in Capaccioli et al. (1993) for the spheroidal component of the galaxy.

The differences in [α/Fe] between major and minor axes are more clearly demonstrated here, as it is evident that at larger radii the major axis data again become consistent with that of the minor axis. This type of behaviour could be understood in terms of changes in the relative contributions of disc and spheroidal components, with both major and minor axes being dominated at small radii by a nuclear component. At intermediate radii, the major axis would be affected by the influence of the disc component, whereas the minor axis would simply be tracing the stellar content of the spheroidal component. The change in the behaviour of the major axis at large radii could then be understood as evidence for truncation of the disc component contribution at around 80 arcsec on the major axis.

The other metallicity tracing indices (Mg b Fe5270 and Fe5335) display similar trends, with slight evidence for breaks in the major axis data at around the same radius as the one seen in [α/Fe]. This has previously been observed by Fisher et al. (1996) in their edge-on sample of S0 galaxies (unfortunately they did not examine the minor axis of NGC 3115), who found that the Mg_2 index is stronger with a

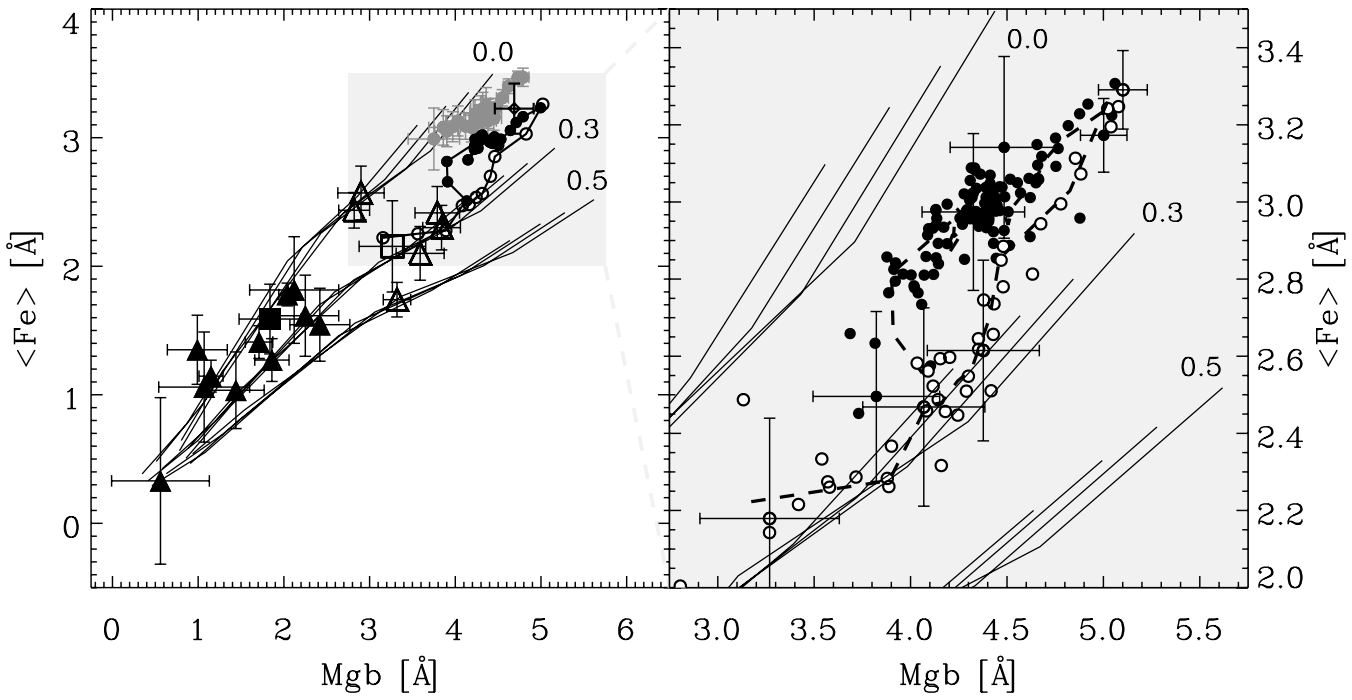

Figure 4. Comparison of the [α/Fe] ratios of the galaxy data and GC population through the use of an Mg b versus $\langle$Fe$\rangle$ diagram. In the left-hand panel, filled and open black circles are binned major and minor axis galaxy data from this paper, filled grey circles show results from Fisher et al. (1996), the open diamond is the central galaxy result from Trager et al. (1998). Filled black triangles are the blue globular cluster sample and unfilled triangles are the red globular cluster sample, both from Kuntschner et al. (2002). Filled black square is the error-weighted mean of the blue cluster subpopulation and the black square the error-weighted mean of the red cluster subpopulation. Over-plotted are models by Thomas et al. (2003, 2004) with abundance ratios [α/Fe] = 0.0, 0.3, 0.5, the models have ages 3–12 Gyr and metallicity [Z/H] = -2.25, -1.35, -0.33, 0.0 and $+0.35$. Right-hand panel shows the unbinned galaxy data presented here, dashed lines denote the positions of the binned data. Representative error bars are plotted for spectra located at small, intermediate and large radii; errors are a combination of bootstrapped 1σ errors and those introduced by a $\pm$5 per cent error in the sky subtraction.

lower gradient at larger radii on the major axis than on the minor axis. As can be seen from Fig. 4, the values for Mg b Fe5270 and Fe5335, determined here for the major axis, are in good agreement with those determined by Fisher et al. (1996). Small differences between the two data sets can be attributed to variations in the experimental set-up, the different methods employed to correct for the broadening effect of the LOSVD and the uncertainty on our correction to the Lick system.

4.3 Age determinations

Fig. 6. examines the behaviour of age-sensitive indices along the major and minor axes of NGC 3115. Model grids are interpolated between the [α/Fe] = 0.0 and 0.3 models from Thomas, Maraston & Bender (2003) and Thomas et al. (2004) with [α/Fe] determined as described previously. Note that whilst the [α/Fe] ratios used to produce the major axis grids are appropriate for the longslit data described here, they are generally not appropriate for the GCs which tend to have mean [α/Fe] $\sim$ 0.3. However, the minor axis grids provide a good approximation to the mean [α/Fe] of the GCs and hence the best age determinations for the clusters.

The Hβ, H$\gamma_{\rm A}$ and H$\delta_{\rm A}$ indices are plotted against [MgFe]$'$ where [MgFe]$' = \sqrt{\rm Mgb \times (0.72 \times Fe5270 + 0.28 \times Fe5335)}$ (Thomas et al. 2003). This index was found by Thomas et al. (2003) to be independent of [α/Fe] and a good tracer of total metallicity.

There appears to be a difference in age between the two axes with the major axis having a mean age of around 5–8 Gyr and the minor axis an age of around 12 Gyr. This would suggest that a small amount of star formation may have continued in the disc component for several Gyr after the formation of the spheroid.

The age determinations from the Hβ index appear to change at lower [Z/H] but in the opposite sense for each axis, with the major axis appearing to become younger and the minor axis older. As Hβ is relatively unaffected by changes in [α/Fe], this cannot be explained as being due to changes in [α/Fe] along either axis, but could be explained for the major axis by more recent star formation in the outer parts of the disc (in spiral arms perhaps). Another possibility would be that some undetected Hβ emission in the inner regions of the disc weakens the observed Hβ index in the inner regions. This final possibility, however, seems unlikely since we find negligible signs of [O III] emission. For the minor axis data, it would seem plausible that the populations at larger radii could be older and would in fact represent the older generation of stars also being traced by the GC populations. This possibility would seem to gain credence from the fact that at larger radii the minor axis data display [α/Fe], ages and [Z/H] values that are entirely consistent with those determined from the red GC subpopulation.

The remaining age estimators H$\gamma_{\rm A}$ and H$\delta_{\rm A}$ also show an age offset between the minor and the major axis in the same sense as Hβ, but there is little or no evidence for an age gradient.

Fig. 7 shows the radial profiles of ages determined by the χ^2 minimization described previously. As should be expected, the trends previously described are obvious with the major axis appearing to have an age of 5–8 Gyr and the minor axis having an age of between 12 and 14 Gyr.

A further comment is that despite the use of different age-sensitive indices, our age determinations for the GCs are entirely consistent

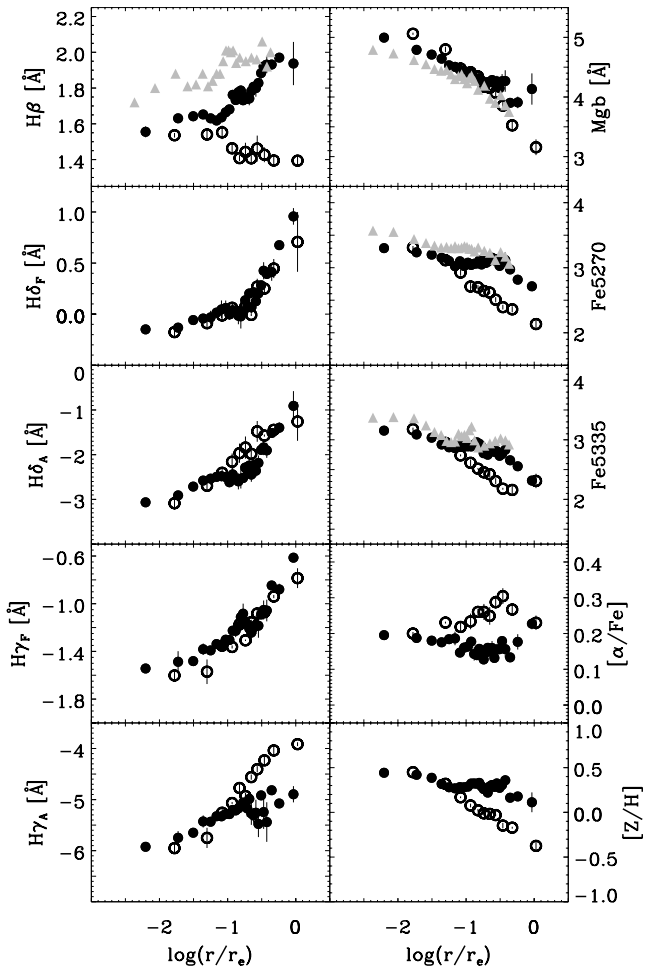

Figure 5. Radial profiles of the Lick indices, [Z/H] and [α/Fe]. [Z/H] and [α/Fe] determined by χ^2 minimization as described in Section 4.1. Filled black circles show major axis data, open circles show minor axis data and light grey triangles show data from Fisher et al. (1996). Error bars are 1σ errors in each bin. Note that $r_e = 93$ and 35 arcsec for the major and minor axes, respectively (Capaccioli et al. 1993).

with those of Kuntschner et al. (2002) with both GC populations having a mean age of around 12 Gyr. In fact, the agreement is now improved as the mean ages of the subgroups determined by Kuntschner et al. (2002) varied from ∼6 to 12 Gyr, depending on the Balmer line being examined. This spread can now be understood as being due to the [α/Fe] sensitivity of the $H\gamma_F$ and $H\delta_F$ lines used in the Kuntschner analysis, which can now be corrected using the newer SSP models provided by Thomas et al. (2004).

5 A SIMPLE TWO-COMPONENT MODEL

To test the hypothesis that radial trends in [α/Fe] could be explained by intrinsic differences in the disc and spheroid components, a simple model was constructed.

The relative contributions of the disc and spheroid components were determined from archived GMOS images of NGC 3115 obtained in 2004 (Program ID GS-2004A-Q-9, PI R.M. Sharples) in the *g*, *i* and *r* bands. The program GALFIT (Peng et al. 2002) was used to carry out a simple bulge to disc decomposition. Because we only wish to know the relative contribution of the two components and we are only interested in a simple first-order model, a full isophotal decomposition was unnecessary and a simple de Vaucouleurs model of the spheroid with $r_e = 93$ arcsec (Capaccioli et al. 1993) was subtracted from the original image to isolate the disc light contribution. As a test of this approach, we also allowed GALFIT to attempt to fit the images with a Sersic function with variable r_e and n, both with and without masking of the disc region and with varying starting parameters. The results in terms of r_e and n varied considerably, but the distribution of flux in the residual image remained fairly constant, with the disc tending to provide a peak of around 30–40 per cent of the flux on the major axis.

The results of this bulge subtraction can be seen in Fig. 8. As previously noted by Capaccioli, Vietri & Held (1988), the disc shows considerable flaring in the outer parts, which these authors attributed to the disc ceasing to be self-gravitating in this region. There is also evidence for structure within the disc (spiral arms?), which could be taken as evidence for some residual star formation events. Note that the inner region is not well fitted by this model. A more realistic model would require several components, but is beyond what is required for the present analysis.

The model can be used to predict [α/Fe] at any point, if it is assumed that the residual light traces an enriched disc and nuclear component with [α/Fe] ~ 0.0 and that the fitted spheroid traces a lower Fe-enriched population of [α/Fe] ~ 0.3. By weighting the [α/Fe] value by the relative fractions of the two components, it is possible to estimate the observed [α/Fe] at any point. Fig. 9 shows the result of this procedure for both axes. This simple model reproduces the general trends observed with [α/Fe] quickly rising on the minor axis and a much more Fe-enriched major axis which trends back towards the asymptotic values of the minor axis at large radii. The differences between the model and the observed values can be explained by a number of factors including incorrect values for the intrinsic [α/Fe] of the two components and the effect of other unaccounted for components. Other factors such as intrinsic gradients in [α/Fe] could also play a part. However, to first order we believe that differences in [α/Fe] between the two axes of NGC 3115 can be explained as being due to the existence of at least two distinct stellar populations within the galaxy, with different spatial distributions and enrichment histories.

6 DISCUSSION

In general, all of our kinematical measurements are in good agreement with previous studies, the most interesting finding being that the disc of the galaxy is particularly cold ($\upsilon_{\rm disc}/\sigma_{\rm disc} > 2$) and hence rotationally supported. An interesting extension to this work would be to improve the statistics of the kinematics beyond 100 arcsec, which would probe the region where substantial flaring of the disc has been observed. The fact that the rotation velocity on the major axis remains high even at large radii where the integrated light is dominated by the underlying spheroid implies that in NGC 3115 the halo is also rotating significantly ($\upsilon/\sigma \sim 1.5$) in the same sense as the disc.

We have confirmed that the GC population shows clear evidence for rotation, in the same sense as that of the disc. Statistics on the GC kinematics at present are not sufficient to associate particular cluster populations to any specific structural feature.

Our investigation of the Lick absorption-line indices has shown that the stellar disc component is considerably different from the spheroidal component in almost all measured parameters. Most informative in terms of constraints on formation theories is the implication that the disc of the NGC 3115 is several Gyr younger, and significantly enriched in metals, compared to the spheroid of the galaxy. This has been hinted at previously by studies of the optical colours

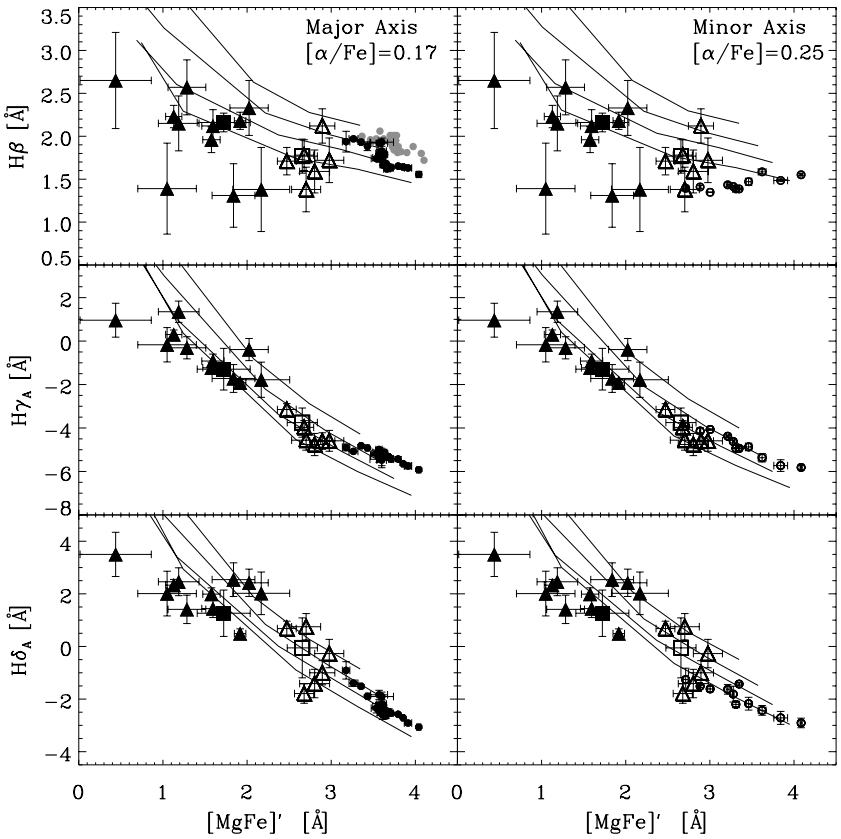

Figure 6. Age–metallicity diagnostic plots for major and minor axis data. Symbols are as in Figure 4. Over-plotted are models by Thomas et al. (2003, 2004) with abundance ratios [α/Fe] indicated in the top right corner of each column; a value of [α/Fe] = 0.25 was chosen for the minor axis as an average of the values determined at small and large radii. These [α/Fe] ratios are interpolated from the 0.0 and 0.3 values listed in Thomas et al. (2004), the models have metallicity [Z/H] = -2.25 to $+0.35$, lines indicate ages from top to bottom of 3, 5, 8 and 12 Gyr, respectively. Error bars for galaxy data are the 1σ errors on each of the radial bins.

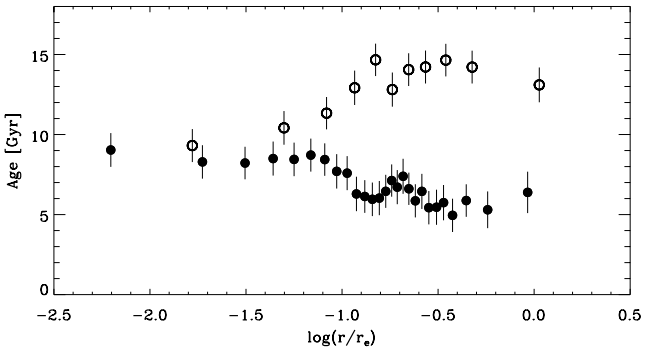

Figure 7. Radial profiles of measured age for major and minor axes. Ages determined by χ^2 minimization as described in Section 4.1. Symbols as previously defined.

of NGC 3115, for example, Silva et al. (1989), who noted that in $B - i$ the disc was 0.5-mag bluer than the spheroid. This colour difference, however, could be attributed either to a younger stellar population in the disc or to the disc having a lower metal abundance compared to the spheroid. We have convincingly demonstrated that a lower metal abundance cannot explain this colour difference since the major axis displays a *higher metal abundance* than that of the minor axis. The difference in colour can therefore clearly be attributed to an age difference of 5–7 Gyr for the two components and is also consistent with the observation that [α/Fe] ratios are lower on the inner region of the major axis.

The red GC subpopulation is most consistent with the larger radii minor axis data in its measured parameters. This suggests that both the spheroid and the red GC population may have formed from the same material at around the same time. An interesting extension would be to probe to larger radii to see if the observed trends in metallicity and [α/Fe] shown in Fig. 5 continue, and eventually lead to the minor axis spheroid data tracing stellar populations similar to those that make up the lower metallicity blue GC population. This blue population of GCs could then possibly be attributed to an initial burst of star formation during the halo formation of the galaxy. One unanswered question is whether or not there exists a GC population associated with the substantial younger disc component of this galaxy. At present, the number of GCs for which spectroscopy exists is too small to exclude this possibility. Though at present none of the GCs examined has line-strength indices comparable to those measured for the disc component. If no such population exists, this in itself would prove interesting as it would imply that GCs are not necessarily formed whenever a sizeable amount of star formation occurs.

7 CONCLUSIONS

We have presented new kinematical data and absorption line-strength measurements for the major and minor axes of the S0

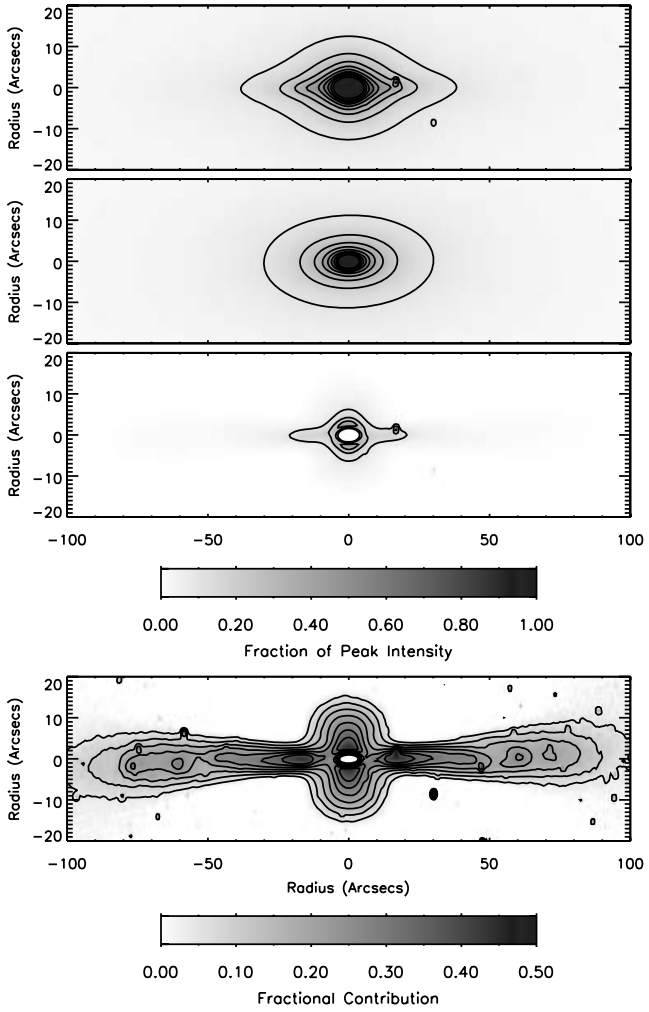

Figure 8. Top image shows original GMOS *i* band image. The second image shows the simple de Vaucouleurs model for the spheroidal component. The third image shows the residual image after the second is subtracted from the first. These three images are all scaled to the peak intensity of the original image for clarity. Contours show the 0.1, 0.2, 0.3, 0.4, 0.5, 0.6, 0.7, 0.8, 0.9 fractions. The lower image shows the fraction of the total emission provided by the residual components. Considerable flaring of the disc is visible, as is substructure consistent with spiral arm structures. Contours show the 0.1, 0.2, 0.3, 0.4 and 0.5 fractions.

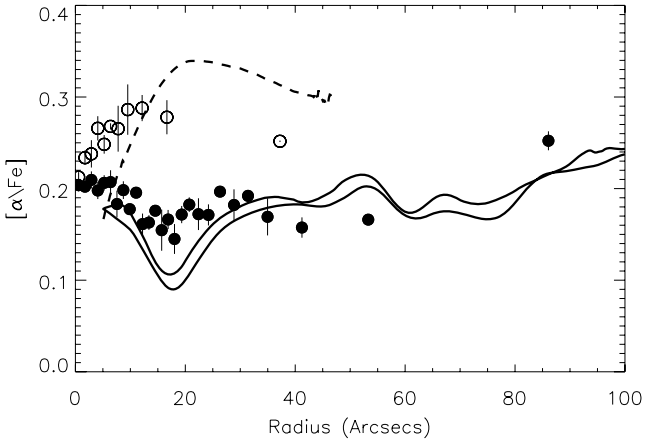

Figure 9. Model predictions for variation of [α/Fe] for major and minor axes. Solid line shows the model prediction for the major axis, dashed line displays the model prediction for the minor axis, both made assuming [α/Fe] = 0.0 for the disc and 0.3 for the spheroid. The circles show radially binned [α/Fe] measurements shown previously in Fig. 5 for the respective axes. Slight differences between both the sides of the major axis are visible in the model predictions, which have been folded about the centre.

galaxy NGC 3115, and have compared these measurements to similar data for the GC system of NGC 3115. Our main conclusions are as follows.

(i) NGC 3115 has a significant stellar disc component, which is both kinematically and chemically distinct from the surrounding spheroidal component.

(ii) The spheroidal component of NGC 3115 is consistent with having a uniformly old ∼10–12 Gyr age and [α/Fe] of 0.2–0.3. At large radii, the minor axis (which should trace the spheroidal component exclusively beyond the central few arcsec) is consistent in age, [α/Fe] and metallicity with the red GC subpopulation, hinting at a common origin for the two.

(iii) The major axis data display clear evidence for contamination by a younger (5–8 Gyr old), more chemically enriched stellar disc. The observation that the disc of NGC 3115 is bluer than the spheroid is primarily an age difference not a metallicity difference effect.

(iv) Previously observed discrepancies in age determination between the Hβ and higher order Balmer lines for the GC sample can largely be explained by changes in the higher order Balmer lines due to varying [α/Fe].

(v) The GC system displays clear evidence for prograde rotation in the same sense as the disc and spheroidal components.

ACKNOWLEDGMENTS

The authors would like to thank Mark Swinbank and Jim Geach for their useful input and discussions. We also thank the anonymous referee for several suggestions which improved the presentation of this paper. MAN acknowledges financial support from PPARC.

This work is based on observations obtained at the Gemini Observatory, which is operated by the Association of Universities for Research in Astronomy, Inc., under a cooperative agreement with the NSF on behalf of the Gemini partnership: the National Science Foundation (United States), the Particle Physics and Astronomy Research Council (United Kingdom), the National Research Council (Canada), CONICYT (Chile), the Australian Research Council (Australia), CNPq (Brazil) and CONICET (Argentina).

REFERENCES

Bender R., Saglia R. P., Gerhard O. E., 1994, MNRAS, 269, 785
Capaccioli M., Cappellaro E., Held E. V., Vietri M., 1993, A&A, 274, 69
Capaccioli M., Vietri M., Held E. V., 1988, MNRAS, 234, 335
Cappellari M., Emsellem E., 2004, PASP, 116, 138
Elson R. A. W., 1997, MNRAS, 286, 771
Emsellem E., Dejonghe H., Bacon R., 1999, MNRAS, 303, 495
Fisher D., 1997, AJ, 113, 950
Fisher D., Franx M., Illingworth G., 1996, ApJ, 459, 110
González J. J., 1993, PhD thesis Univ. California at Santa Cruz
Hook I. M., Jørgensen I., Allington-Smith J. R., Davies R. L., Metcalfe N., Murowinski R. G., Crampton D., 2004, PASP, 116, 425
Illingworth G., Schechter P. L., 1982, ApJ, 256, 481
Jones L. A., 1997, PhD thesis, Univ. North Carolina, Chapel Hill

Kavelaars J. J., 1998, PASP, 110, 758
Kormendy J., Richstone D., 1992, ApJ, 393, 559
Kundu A., Whitmore B. C., 1998, AJ, 116, 2841
Kuntschner H., 2000, MNRAS, 315, 184
Kuntschner H., 2004, A&A, 426, 737
Kuntschner H., Ziegler B. L., Sharples R. M., Worthey G., Fricke K. J., 2002, A&A, 395, 761
Michard R., Marchal J., 1994, A&AS, 105, 481
Peng C. Y., Ho L. C., Impey C. D., Rix H.-W., 2002, AJ, 124, 266
Proctor R. N., Forbes D. A., Beasley M. A., 2004, MNRAS, 355, 1327
Puzia T. H., Zepf S. E., Kissler-Patig M., Hilker M., Minniti D., Goudfrooij P., 2002, A&A, 391, 453
Puzia T. H. et al., 2004, A&A, 415, 123
Puzia T. H., Kissler-Patig M., Thomas D., Maraston C., Saglia R. P., Bender R., Goudfrooij P., Hempel M., 2005, A&A, 439, 997
Schlegel D. J., Finkbeiner D. P., Davis M., 1998, ApJ, 500, 525
Silva D. R., Boroson T. A., Thompson I. B., Jedrzejewski R. I., 1989, AJ, 98, 131
Thomas D., Maraston C., Bender R., 2003, MNRAS, 339, 897
Thomas D., Maraston C., Korn A., 2004, MNRAS, 351, L19
Trager S. C., Worthey G., Faber S. M., Burstein D., Gonzalez J. J., 1998, ApJS, 116, 1
Vazdekis A., 1999, ApJ, 513, 224
Worthey G., Ottaviani D. L., 1997, ApJS, 111, 377

SUPPLEMENTARY MATERIAL

The following supplementary material is available for download as part of the full-text version of the article from http://www.blackwell-synergy.com.

Table 3. NGC 3115 major axis kinematics from Norris, Sharples & Kuntschner (2006).

Table 4. NGC 3115 minor axis kinematics from Norris, Sharples & Kuntschner (2006).

Table 5. NGC 3115 major axis ages, metallicities, abundance ratios and Lick indices from Norris, Sharples & Kuntschner (2006).

Table 6. NGC 3115 minor axis ages, metallicities, abundance ratios and Lick indices from Norris, Sharples & Kuntschner (2006).

This paper has been typeset from a TEX/LATEX file prepared by the author.